7. Kyotani, T., Tsai, L.-F. & Tomita, A. Formation of platinum nanorods and nanoparticles in uniform carbon nanotubes prepared by a template carbonization method. *Chem. Commun.* 701–702 (1997).
8. Dahu, J. R., Zheng, T., Liu, Y. & Xue, J. S. Mechanisms for lithium insertion in carbonaceous materials. *Science* **270,** 590–593 (1995).
9. Sato, K., Noguchi, M., Demachi, A., Oki, N. & Endo, M. A mechanism of lithium storage in disorder carbons. *Science* **264,** 556–558 (1994).
10. Freemantle, M. Filled carbon nanotubes could lead to improved catalysts and biosensors. *Chem. Eng. News* **74,** 62 (1996).
11. Baum, R. M. Nurturing nanotubes, remarkable properties of nanotubes suggest range of new technologies; workshop examines how to develop them. *Chem. Eng. News* **75,** 39–41 (1997).
12. Dillon, A. C. *et al.* Storage of hydrogen in single-walled carbon nanotubes. *Nature* **386,** 377–379 (1997).
13. Gadd, G. E. *et al.* The world's smallest gas cylinders. *Science* **277,** 933–936 (1997).
14. Planeix, J. M. *et al.* Application of carbon nanotubes as supports in heterogeneous catalysis. *J. Am. Chem. Soc.* **116,** 7935–7936 (1994).
15. Sloan, J., Cook, J., Green, M. L. H., Hutchison, J. L. & Tenne, R. Crystallisation inside fullerene related structures. *J. Mater. Chem.* **7(7),** 1089–1095 (1997).
16. Wong, S. S., Harper, J. D., Lansbery, P. T. & Lieber, C. M. Carbon nanotube tips: High-resolution probes for imaging biological systems. *J. Am. Chem. Soc.* **120,** 603–604 (1998).
17. Dai, H. J., Hafner, J. H., Rinzler, A. G., Colbert, D. T. & Smalley, R. E. Nanotubes as nanoprobes in scanning probe microscopy. *Nature* **384,** 147–150 (1996).
18. Li, W. Z. *et al.* Large-scale synthesis of aligned carbon nanotubes. *Science* **274,** 1701–1703 (1996).
19. Nishizawa, M., Mukai, K., Kuwabata, S., Martin, C. R. & Yoneyama, H. Template synthesis of polypyrrole-coated spaniel $LiMn_2O_4$ nanotubules and their properties as cathode active materials for lithium batteries. *J. Electrochem. Soc.* **144,** 1923–1927 (1997).
20. Che, G., Jirage, K. B., Fisher, E. R., Martin, C. R. & Yoneyama, H. Chemical-vapor deposition-based template synthesis of microtubular TiS_2 battery electrodes. *J. Electrochem. Soc.* **144,** 4296–4302 (1997).
21. Jean, M., Desnoyer, C., Tranchant, A. & Messina, R. Electrochemical and structural studies of petroleum coke in carbonate-based electrolytes. *J. Electrochem. Soc.* **142,** 2122–2125 (1995).
22. Verbrugge, M. W. & Koch, B. J. Lithium intercalation of carbon-fiber microelectrodes. *J. Electrochem. Soc.* **143,** 24–31 (1996).
23. Bockris, J. O'M. & Srinivasan, S. *Fuel Cells: their Electrochemistry* (McGraw-Hill, New York, 1969).
24. Bard, A. J. & Faulkner, L. R. *Electrochemical Methods, Fundamentals and Applications* (Wiley, New York, 1980).
25. Ye, S., Uijh, A. K. & Dao, L. H. A new fuel cell electrocatalyst based on highly porous carbonized polyacrylonitrile foam with low platinum loading. *J. Electrochem. Soc.* **143,** L7–L9 (1996).
26. Shen, P. K. & Tseung, A. C. C. Anodic oxidation of methanol on Pt/WO_3 in acidic media. *J. Electrochem. Soc.* **141,** 3082–3089 (1994).

Acknowledgements. This work was supported by the US Department of Energy and the US Office of Naval Research.

Correspondence and requests for materials should be addressed to C.R.M. (e-mail: crmartin@lamar.colostate.edu).

Entropically driven microphase transitions in mixtures of colloidal rods and spheres

Marie Adams*, Zvonimir Dogic*, Sarah L. Keller† & Seth Fraden*

* *The Complex Fluids Group, Martin Fisher School of Physics, Brandeis University, Waltham, Massachusetts 02254, USA*
† *Department of Chemical Engineering, University of California, Santa Barbara, California 93106, USA*

Although the idea that entropy alone is sufficient to produce an ordered state is an old one in colloid science[1], the notion remains counter-intuitive and it is often assumed that attractive interactions are necessary to generate phases with long-range order. The phase behaviour for both rods and spheres has been studied experimentally[1–7], theoretically[8,9] and by computer simulations[10]. Here we describe the phase behaviour of mixtures of colloidal rod-like and sphere-like particles (respectively viruses and polystyrene latex or polyethylene oxide polymer) under conditions in which they act like hard' particles[2,3]. We find a wealth of behaviour: bulk demixing into rod-rich and rod-poor phases and microphase separation into a variety of morphologies. One microphase consists of layers of rods alternating with layers of spheres[11]; in another microphase of unanticipated complexity, the spheres reversibly assemble into columns, which in turn pack into a crystalline array. Our experiments, and previous theory and computer simulations[11], suggest that this phase behaviour is entropically driven by steric repulsion between particles. The phenomena are likely to be quite general, applying also for example to low-molecular-mass liquid crystals[12]. This kind of microphase separation might also be relevant to systems of amphiphiles[13] and block copolymers[14], to bioseparation methods and DNA partitioning in prokaryotes[15], and to protein crystallization[16,17] and the manufacture of composite materials.

The phase behaviour of a colloidal suspension is found by minimizing the free energy $F = U - TS$. Hard particles are forbidden to interpenetrate and the interaction energy U is zero as long as the particles are not in contact. Thus phase behaviour is determined by maximizing the entropy S. For hard spheres, imagine a suspension of billiard balls, and for hard rods substitute billiard cues. Examples of entropically driven ordering exhibited by hard rods are the nematic and smectic liquid-crystalline phases, whereas for hard spheres a fluid–crystal transition occurs. These phase transitions have been extensively studied theoretically[8,9], by computer simulations[10], and experimentally in a variety of colloidal systems, including the ones studied here[1–7]. Another class of entropically driven ordering arises in mixtures in which demixing transitions often occur. If one of the physical properties of the individual molecular species, such as shape or flexibility, is different enough, then either bulk or microphase separation will occur for an appropriate composition of the components.

The physical origin of phase separation in hard particle suspensions is both extremely simple and general. The free volume of a suspension composed of a binary mixture of macromolecules is maximized when the two components phase-separate. Increasing the free volume (see insert to Fig. 1) raises the translational entropy of the macromolecules, but at the expense of lowering the entropy of mixing. At low concentrations, the mixing entropy dominates and the solution is miscible, but with increasing concentration, if the gain in free volume is sufficient, phase separation will occur. Although the interparticle potential is purely repulsive, like-components experience an effective attraction. This phenomenon is known by different names—depletion attraction in physics and

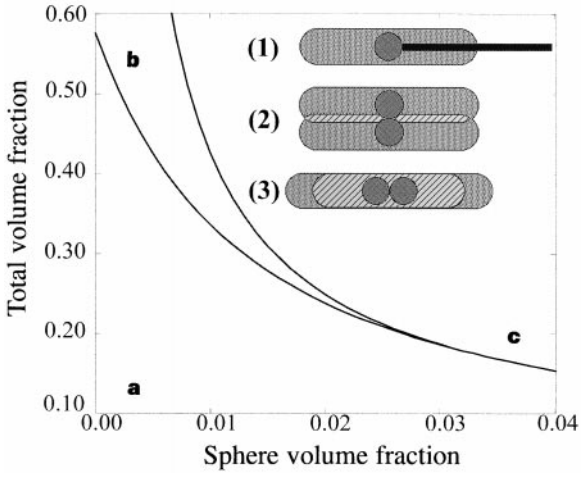

Figure 1 Theoretical phase diagram for aligned spherocylinders of length L, diameter D, and spheres of diameter σ (ref. 11) for $L/D = 100$ and $\sigma/D = 10$. Upon addition of spheres, the total volume fraction needed to form a lamellar phase (**b**) decreases, hence spheres stabilize the smectic phase. In **a**, the rods and spheres are miscible, and in **c**, bulk phase separation occurs. Insert: (1) The volume excluded (light grey) to the centre of a horizontally aligned rod (black) by a sphere (dark grey). (2) Bringing two spheres together in a suspension of parallel rods leads to an overlap of excluded volume (wide cross-hatch)–increasing the free volume and thus the translational entropy of the rod. (3) Aggregation of the spheres parallel to the rods produces more overlap of excluded volume than in insert 2.

chemistry[16,18–24], but is macromolecular crowding in biology[15,25]. Depletion phenomena are general because all particles at any scale possess a hard core that must be considered in any accurate theoretical model. For the case of the colloidal suspensions studied here, hard-core repulsion is the dominant interaction because salt added to the suspension screens electrostatic repulsion.

In our experiments, we either add polyethylene oxide (PEO), polyethylene glycol (PEG) or polystyrene latex (PS) spheres to suspensions of the filamentous bacteriophage fd virus in the isotropic or nematic phases. When low concentrations of spheres that are small compared to the fd length (22 nm diameter PS, 5% volume fraction) are added to a pure fd nematic (20 mg ml^{-1}, 10 mM Tris), we observe bulk phase separation of the rods into an isotropic and nematic phase. The spheres partition into the rod-poor phase in the form of ellipsoidal shaped droplets, with the long axis parallel to the nematic director (rod alignment axis). In contrast, when PS spheres at any concentration larger than about 700 nM are added to the pure fd nematic, complete demixing of the spheres into dense, irregular shaped aggregates elongated along the nematic director is observed.

The full complexity of the phase diagram of rod/sphere mixtures is illustrated in Figs 2 and 3. Upon increasing from zero the concentration of 100-nm-diameter PS spheres in a dilute fd nematic sample, the spheres assemble into columns of ~300 nm diameter that are up to 5 μm long and oriented perpendicular to the rods' long axis. The columns in turn pack on a two-dimensional lattice with diametrically opposed columns approximately two rod-lengths apart. Birefringence measurements indicate no disruption of the alignment of the rods; we call this phase 'columnar'. As the sphere concentration is increased, the columns continuously diminish in diameter and spheres fill in the line joining the two opposite columns that are perpendicular to the rod alignment direction. Eventually the columns disappear and a 'lamellar' phase is formed of a layer of rods alternating with a layer of spheres. Both the lamellar and columnar phases are equilibrium phases; we have one lamellar phase of over two years old.

Freeze-fracture electron microscopy of the lamellar phase (Fig. 3b(2)) revealed cases in which one layer of aligned but disordered rods alternated with a layer of disordered spheres about two diameters thick. This was consistent with optical microscopy (Fig. 3b(1)) results that measured the periodicity of the lamellar phase at 1.1 μm, about 0.2 μm longer than the fd molecule, or twice the diameter of the PS spheres. At higher fd concentrations, filaments of the lamellar phase were observed. Filaments had uniform diameter, but with a variance of diameter among filaments in the same sample, ranging from 2 to 100 μm diameter with lengths of the order of centimetres. Filaments formed within minutes after initially mixing the fd and PS. Samples ranging in age from a day to several months resembled those shown in Fig. 3c, d, but bulk demixing of the rods and spheres occurred after one year. These filaments formed in co-existence with either fd in a nematic phase, or in the smectic phase. The smectic phase had a periodicity of 0.9 μm, identical to that of pure fd suspensions.

The lamellar phase is initially largely defect-free, and at low concentrations is very flexible. Fluorescently labelled spheres are seen to hop between layers. With increasing sphere concentration, the lamellae become rigid and hopping between layers stops. As the sphere concentration is further increased, the number of defects multiply until the size of defect-free regions is only several molecular lengths. Neither swelling of the layers nor bulk phase separation was noted as a function of sphere concentration.

Phase diagrams of identical topology were observed using polystyrene spheres ranging from 22 to120 nm diameter, but the concentration of spheres needed to induce lamellar order increased

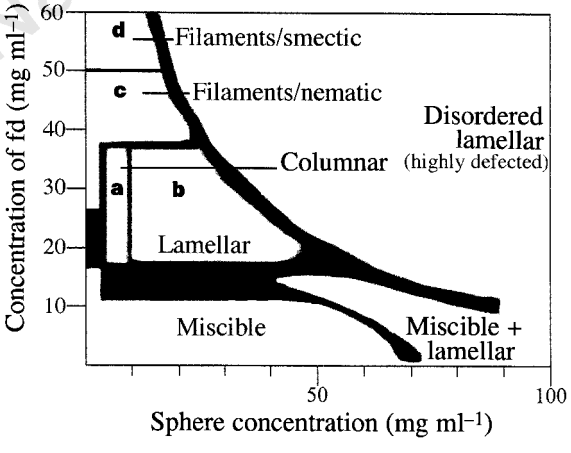

Figure 2 Phase diagram for fd and 100-nm diameter polystyrene spheres. The ionic strength (I) was 5 mM at pH 8.2, but a topologically identical diagram was observed with I = 50 mM. The phase sequence for pure fd (I = 5 mM) is isotropic–nematic at 15 mg ml^{-1} and nematic–smectic at 55 mg ml^{-1} (ref. 6). At volume fractions of spheres as low as 0.5% (5 mg ml^{-1}) and rod concentrations of 20 mg ml^{-1}, far below the smectic phase, we observe microphase separation. The appearance and structure of those phases labelled with letters are shown in Fig. 3.

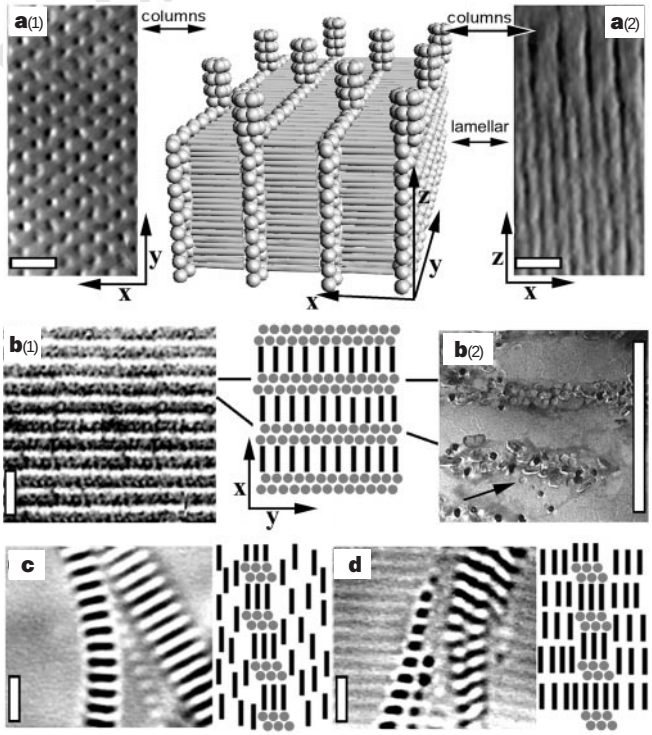

Figure 3 Photographs and diagrams of regions of the phase diagram shown in Fig. 2. Unless specified, photographs are differential interference contrast (DIC) microscopy. The micrographs cannot clearly resolve single particles, so the drawings give only an approximate representation of the structure. The actual volume fraction of the spheres within the columns and lamellae is 10–20%. Length bars are 3 μm. **a**(1), **a**(2), Orthogonal sections of co-existing columnar and lamellar phases. **a**(1), Section in the x–y plane perpendicular to the columns, corresponding to the upper part of the adjacent drawing–each column is about 3 spheres in diameter; **a**(2), section in the x–z plane corresponding to the front of the drawing. The columns (top) have twice the spacing of the lamellae (bottom). The lamellar phase is shown in **b**(1); **b**(2) is a freeze-fracture electron micrograph[28]. The arrow indicates a hemispherical divot where a sphere was lifted out of the plane by the fracturing process. In **c** and **d**, filaments of the lamellar phase (high contrast) co-existing with either the phase separated rods in a nematic of uniform texture (**c**) or smectic with weak contrast (**d**). Filaments are metastable but long-lived structures. The periodicity of the lamellar (1.1 μm) is larger than the periodicity of the smectic (0.9 μm).

with decreasing sphere size. Columnar phases were observed for PS in the 60–120 nm range: notably, the diameter of the columns of spheres remained the same at ~300 nm. The lamellar phase (but not columnar) was also observed with PEO relative molecular mass (M_r) of 8,000K, which has a hydrodynamic radius of 100 nm (ref. 26).

PS spheres of size greater than 250 nm did not form the lamellar phase. When low concentrations of 300-nm-diameter PS spheres were added to fd nematics, we observed rapid association of the spheres into chain-like structures (Fig. 4). At higher densities, the spheres packed into a cubic array with a lattice constant of one rod length.

A microscopic but highly simplified theory models the fd as perfectly aligned hard rods, the PS as hard spheres, and treats interactions at the second-virial level[11]. We have used this theory to calculate the stability limits of the phase diagram (Fig. 1). This predicts topologically identical phase diagrams for all sphere diameters. The experimental phase diagrams were remarkably similar to theory for spheres ranging in diameter from 22 to 200 nm. However, above this sphere diameter no lamellar phase is seen, in contrast to theory. The theory also predicts swelling of the layers, in contrast to experiment, and furthermore, the theory does not account for the columnar phase.

The observed lamellar and columnar phases in fd/PS mixtures bear strong resemblance to micellar[13] and block-copolymer[14] systems, in which microphase ordering is driven by the tendency of the antagonistic (or amphiphilic) portions of an individual molecule to phase separate while being prevented from doing so by chemical bonds. In contrast, no bonds exist between the rods (fd) and spheres (PS), so naively we expect bulk demixing of rods and spheres[23,24]. The photograph in Fig. 4 of 300-nm spheres immersed in a nematic suspension of fd rods suggests an explanation of why the lamellar phase is preferred to bulk demixing of the rods and spheres[23,24]. The photographs indicate 300-nm spheres have two preferred configurations: either spheres in contact or separated by one rod length, which suggests that these are low-energy configurations. In other words, the pictures demonstrate that in a rod–sphere mixture there is an effective sphere–sphere attraction (promoting bulk phase separation) and an effective rod–sphere attraction (promoting microphase formation). Depletion theory explains the sphere–sphere association as a way to maximize free volume, and hence total entropy. We speculate that the rod–sphere attraction arises from correlations among the rods induced by the presence of spheres (Fig. 4). These experiments and theoretical arguments demonstrate that the bond linking the two portions of a co-polymer is not essential for inducing microphase ordering, contrary to conventional wisdom[13,14].

Although there is partial understanding of the lamellar phase, the columnar phase remains a mystery and presents a theoretical challenge. Analysis of the phenomena described here is relevant to both the high-molecular-mass macromolecules used in this study, as well as low-molecular-mass ones for which interparticle attractions are significant, because all molecules possess a repulsive steric core. Thus the entropic forces discussed here need to be considered in order to have a complete description of the phase behaviour of any mixture containing anisotropically shaped molecules. Furthermore, we have shown that effective attractive potentials of surprising complexity can be constructed through the choice of the shape, size and number of molecules in a suspension, indicating the possibility of manipulating these variables[16,22] to 'engineer with entropy', building order from disorder[21]. □

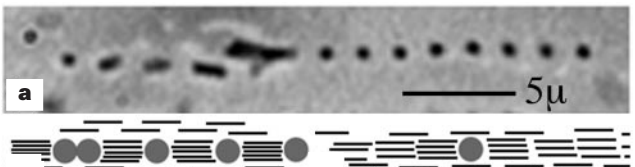

Figure 4 Effective rod–sphere attraction. **a**, DIC micrograph of 300-nm PS spheres in a nematic fd sample. **b**, The spheres either aggregate in close-packed chains (Fig. 1, insert 3) or into open chains in which each sphere is separated by a rod length (0.9 μm). **c**, An interface perpendicular to the nematic alignment direction forces the ends of the rods into registry, setting off a smectic density wave that decays away from the interface. Consequently, slightly more than one rod length away from the sphere the density of rods is lower than average and thus it is easier to insert a second sphere. Such spheres strongly stabilize the lamellar phase (Fig. 1).

Methods

The colloidal rods consist of filamentous bacteriophage fd virus, a semiflexible polymer of 6.6 nm diameter, 880 nm contour length, 2.2 μm persistence length, and negative charge density of 10 e^- per nm (refs 2, 27). Growth and purification of the virus were done using standard methods[2]. The spherical colloids consisted of either monodisperse polystyrene latex spheres, solid charged spheres ranging in diameter from 22 nm to 1.0 μm (Bangs Labs, 1DC), or one of either of the water-soluble neutral polymers; polyethylene glycol or polyethylene oxide of relative molecular masses ranging from 8K to 8,000K (Aldrich, Fluka, Sigma). Colloids were suspended in either 10 mM or 100 mM Tris buffer at pH 8.2 (ionic strength, 5 mM or 50 mM, respectively). Samples were flame-sealed in rectangular glass capillaries of 50 μm path length (Vitro Dynamics).

Phase diagrams were determined by direct observation with differential interference contrast (DIC) and polarizing microscopy on a Nikon MicroPhot SA connected to a MTI CCD-72 video camera and a Scion AG-5 video Frame Grabber interfaced with a MacIntosh computer running NIH Image.

Received 20 January; accepted 30 March 1998.

1. Forsyth, P. A. Jr, Marcelja, S., Mitchell, D. J. & Ninham, B. W. Ordering in colloidal systems. *Adv. Coll. Int. Sci.* **9,** 37–60 (1978).
2. Fraden, S. in *Observation, Prediction, and Simulation of Phase Transitions in Complex Fluids* (eds Baus, M., Rull, L. F. & Ryckaert, J. P.) 113–164 (Kluwer Academic, Dordrecht, 1995).
3. Poon, W. C. K. & Pusey, P. N. in *Observation—Prediction, and Simulation of Phase Transitions in Complex Fluids* (eds Baus, M., Rull, L. F. & Ryckaert, J. P.) 3–51 (Kluwer Academic, Dordrecht, 1995).
4. Tang, J. & Fraden, S. Isotropic–cholesteric phase transition in colloidal suspensions of filamentous bacteriophage fd. *Liq. Cryst.* **19,** 459–467 (1995).
5. Tang, J. & Fraden, S. Temperature dependence of the flexibility of fd: Behavior of the isotropic–cholesteric phase boundary and magnetic birefringence. *Biopolymers* **39,** 13–22 (1996).
6. Dogic, Z. & Fraden, S. Smectic phase in a colloidal suspension of semiflexible virus particles. *Phys. Rev. Lett.* **78,** 2417–2420 (1997).
7. Sato, T. & Teramoto, A. Concentrated solutions of liquid-crystalline polymers. *Adv. Polym. Sci.* **126,** 85–161 (1996).
8. Onsager, L. The effects of shape on the interaction of colloidal particles. *Ann. NY Acad. Sci.* **51,** 627–659 (1949).
9. Hosino, M., Nakano, H. & Kimura, H. Nematic-smectic transition in an aligned rod system. *J. Phys. Soc. Jpn* **46,** 1709–1715 (1979).
10. Frenkel, D. in *Liquids, Freezing, and Glass Transition* (eds Hansen, J. P., Levesque, D. & Zinn-Justin, J.) Ch. 9, 689–762 (Elsevier Science, Amsterdam, 1991).
11. Koda, T., Numajiri, M. & Ikeda, S. Smectic-A phase of bidisperse system of parallel hard rods and hard spheres. *J. Phys. Soc. Jpn* **65,** 3551–3556 (1996).
12. Rieker, T. P. Organic lyotropic lamellar liquid crystals. *Liq. Cryst.* **19,** 497–500 (1995).
13. Gelbart, W. M., Ben-Shaul, A. & Roux, D. (eds) *Micelles, Membranes, Microemulsions, and Monolayers* (Springer, New York, 1994).
14. Bates, F. S. Polymer–polymer phase behavior. *Science* **251,** 898–905 (1991).
15. Walter, H. & Brooks, D. E. Phase separation in cytoplasm, due to macromolecular crowding, is the basis for microcompartmentation. *FEBS Lett.* **361,** 135–139 (1995).
16. ten Wolde, P. R. & Frenkel, D. Enhancement of protein crystal nucleation by critical density fluctuations. *Science* **277,** 1975–1978 (1997).
17. Adams, M. & Fraden, S. Phase behavior of mixtures of rods (tobacco mosaic virus) and spheres (polyethylene oxide, bovine serum albumin). *Biophys. J.* **74,** 669–677 (1998).
18. Asakura, S. & Oosawa, F. Interaction between particles suspended in solutions of macromolecules. *J. Polym. Sci.* **33,** 183–192 (1958).
19. Flory, P. J. Statistical thermodynamics of mixtures of rodlike particles. 5. Mixtures with random coils. *Macromolecules* **11,** 1138–1141 (1978).
20. Gast, A. P., Russel, W. B. & Hall, C. K. An experimental and theoretical study of phase transitions in the polystyrene latex and hydroxyethylcellulose system. *J. Coll. Int. Sci.* **109,** 161–171 (1986).
21. Frenkel, D. in *Proceedings of the Sitges Conference on Complex Liquids* (ed. Garrido, L.) 137–148 (Springer, New York, 1993).
22. Dinsmore, A. D., Yodh, A. G. & Pine, D. J. Entropic control of particle motion using passive surface microstructures. *Nature* **383,** 239–242 (1996).
23. Lekkerkerker, H. N. W. & Stroobants, A. Phase behaviour of rod-like colloid + flexible polymer mixtures. *Il Nuovo Cimento* **16 D** 949–962 (1994).
24. Bolhuis, P., Stroobants, A., Frenkel, D. & Lekkerkerker, H. N. W. Numerical study of the phase behavior of rodlike colloids with attractive interactions. *J. Chem. Phys.* **107,** 1551–1564 (1997).
25. Herzfeld, J. Entropically driven order in crowded solutions: From liquid crystals to cell biology. *Acc. Chem. Res.* **29,** 31–37 (1996).

26. Devanand, K. & Selser, J. C. Polyethylene oxide does not necessarily aggregate in water. *Nature* **343,** 739–741 (1990).
27. Model, P. & Russel, M. in *The Bacteriophages* (ed. Calender, R.) Ch. 6, 375–456 (Plenum, New York, 1988).
28. Chiruvolu, S., Naranjo, E. & Zasadzinski, J. A. *Microstructure of Complex Fluids by Electron Microscopy* (Am. Chem. Soc., Washington DC, 1994).

Acknowledgements. We acknowledge grant support from the NSF (D.M.R.)

Correspondence and requests for materials should be addressed to S.F. (e-mail: seth@smectic.elsie.brandeis.edu). Further information is available on the World Wide Web at http://www.elsie.brandeis.edu.

Low argon solubility in silicate melts at high pressure

Eva Chamorro-Pérez*, Philippe Gillet*, Albert Jambon†, James Badro* & Paul McMillan*‡

** Institut Universitaire de France, Laboratoire de Science de la Terre, CNRS UMR 5570, École Normale Supérieure de Lyon, 46 allée d'Italie, 69364 Lyon cedex 07, France*
† Laboratoire MAGIE, CNRS URA 1762, Université de Paris VI, 4 place Jussieu, 75252 Paris cedex 05, France

The solubility of rare gases in silicate melts and minerals at high pressure is of importance for understanding the early history of the Earth and its present day degassing. Helium, neon, argon, krypton and xenon were originally incorporated into the Earth during its accretion, and have also been produced by radioactive decay[1]. These elements have been used as tracers for deciphering mantle structure and constraining the number and size of geochemical reservoirs[1–3]. In particular, it has been proposed that the budget of ^{40}Ar, produced by the radioactive decay of ^{40}K, provides the strongest argument for chemical layering within the mantle[1,4]. The geochemical models used to arrive at this conclusion are, however, currently under re-examination[5], with a large source of uncertainty being the lack of data on argon partitioning during melting. It has previously been assumed, on the basis of low-pressure data, that noble gases are highly soluble in melts at all pressures. But here we present solubility data of argon in olivine melt at very high pressure that indicate that argon solubility is strongly dependent on pressure, especially in the range of 4–5 gigapascals.

Degassing throughout Earth history has taken place by melting accompanied by dissolution of noble gases in the melt, followed by ascent of melt and escape to the atmosphere. Several recent studies have focused on rare-gas solubility in melts at low pressure (below 2.5 GPa)[6–8]. Newly developed high-pressure diamond anvil cell (DAC) techniques now permit melting experiments on mantle materials in the presence of argon under deep-mantle conditions[9]. Preliminary experiments on pure SiO_2 melt yielded the surprising result that Ar solubility decreased markedly above 5 GPa. We have now obtained data for a natural olivine melt composition that provide a more realistic model for mantle melts.

Polished $100 \times 100 \times 20\ \mu m^3$ plates (Fig. 1a) of single crystalline San Carlos olivine (chemical composition 49wt% MgO, 41wt% SiO_2, 10wt% FeO) were loaded into a high-pressure DAC along with Ar as pressure medium[9]. Pressure was measured from the calibrated shift of the intense Raman lines of the crystal before heating[10]. This avoided a potential chemical reaction with the ruby chips usually used for pressure measurement. Samples were heated at pressures up to 11 GPa by using a focused CO_2 laser beam[11]. Forsterite melts congruently to at least 12.7 GPa (ref. 12). Melting was detected optically by the formation of droplets (Fig. 1b). The laser power was

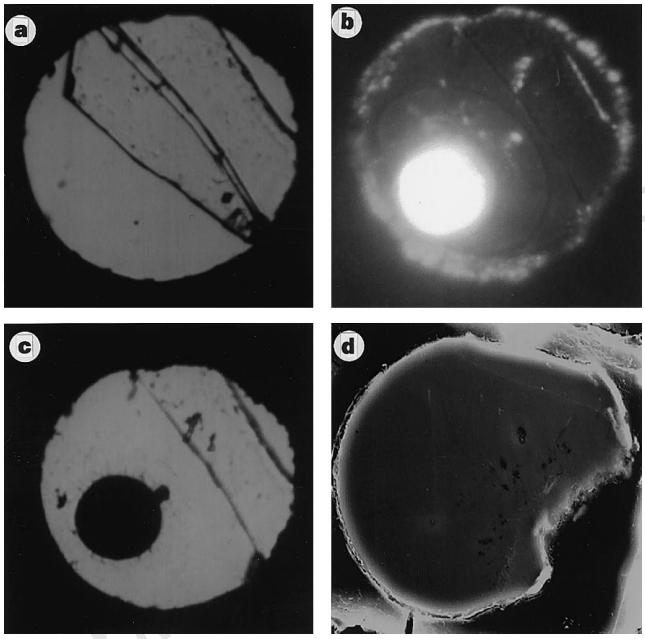

Figure 1 Series of optical micrographs taken through the diamonds of the DAC before and during the laser-heated experiment showing different stages of the high-pressure melting of olivine in the presence of Ar. **a**, Polished single-crystalline slab of San Carlos olivine compressed in solid Ar at 2.5 GPa before heating. The dark outline indicates the gasket hole in the diamond cell experiment. The largest dimension of the sample is 150 μm. The sample edges were fixed at two points of contact to the interior of the metal gasket. At ambient temperature and above 1.2 GPa, the Ar pressure-transmitting medium is solid. The line traversing the sample along its longest dimension is a fracture that occurred during compression. **b**, Photomicrograph of the sample *in situ* during laser heating at 2.5 GPa. The laser power was adjusted so that the temperature inside the molten spot was approximately 100–200 °C above the melting point. Only one piece of the fractured sample has melted to a spherical drop, and has moved away from the other half of the crystal (darker area above the melted spot). A rim of molten argon is visible around the hot bead of olivine melt: the Ar is solid elsewhere. **c**, Photomicrograph of the sample in the DAC after heating. When the laser power is cut, the molten sample quenches rapidly to glass (verified by polarized optical microscopy and micro-Raman spectroscopy, and by SEM analysis of the etched surface after removal from the DAC; see the text). The quenched bead of glassy sample droplet is then decompressed and prepared for chemical analysis. **d**, SEM image of a typical polished sample after etching (1 min in 1 M HCl). The sample surface shows only a smooth glassy texture. No fracture lines or bubbles are observed in the regions that were subjected to chemical analysis with the electron microprobe. The Ar content was measured by energy-dispersive and wavelength-dispersive analysis in the electron microprobe (Cameca SX50) with an accelerating voltage of 15 kV, a beam current of 100 nA and a counting time of 10 s on peak and background. The standard used was an SiO_2 glass containing 1wt% Ar. The Ar signal was measured simultaneously with two spectrometers. The electron beam was defocused to 5 μm in diameter to improve counting statistics on the low rare-gas content. The beam was rastered automatically across the sample surface in 5 μm steps. The reported Ar contents represent an average of approximately 20 points, depending on the sample analysed. A few empty 'bubbles' are visible on the right side of this sample: these are areas where the molten sample was 'pulled away' from the crystalline olivine during initial heating. These areas were avoided during the chemical analyses. All glassy samples analysed in this study formed monolithic blocks that remained intact during removal from the DAC, mounting in epoxy, and polishing. There was no evidence for microcracks or bubbles that might indicate decrepitation, for any of the glassy samples described here. Etching the sample surface did not reveal any additional texture that might indicate the presence of grain boundaries or other features associated with crystallization during the quench. Micro-Raman spectra of quenched samples occasionally showed the two most intense peaks of crystalline olivine superimposed on the broad bands of the glassy sample; however, these were not present for all samples, and there was no systematic difference between samples with high and low Ar content.

‡ Present address: Department of Chemistry and Biochemistry and Center for Solid State Science, Arizona State University, Tempe, Arizona 852287, USA.